An Integrative Model of Insect Flight Control

William B. Dickson * Andrew D. Straw * Christian Poelma *

Michael H. Dickinson †

California Institute of Technology, 1200 E. California Boulevard, Pasadena, CA, 91125, US

This paper presents a framework for simulating the flight dynamics and control strategies of the fruit fly *Drosophila melanogaster*. The framework consists of five main components; an articulated rigid-body simulation, a model of the aerodynamic forces and moments, a sensory systems model, a control model, and an environment model. In the rigid-body simulation the fly is represented by a system of three rigid-bodies connected by a pair of actuated ball-joints. At each instant of the simulation, the aerodynamic forces and moments acting on the wings and body of the fly are calculated using an empirically derived quasi-steady model. The pattern of wing kinematics is based on data captured from high-speed video sequences. The forces and moments produced by the wings are modulated by deforming the base wing kinematics along certain characteristic actuation modes. Models of the fly's visual and mechanosensory systems are used to generate inputs to a controller that sets the magnitude of each actuation mode, thus modulating the forces produced by the wings. This simulation framework provides quantitative test-bed for examining the possible control strategies employed by flying insects. Examples demonstrating visual and mechanosensory based pitch rate, velocity, altitude and flight speed control, as well as visually guided flight down a tunnel, are presented.

I. Introduction

Flight, like all forms of locomotion, involves a complex interaction between an animal and its environment. Although neural circuits, muscles, and wings make up the central physical plant of an animal's motor system, flight behavior does not result from a simple set of feed-forward commands. For example, most of an insect's nervous system is dedicated to the sensory information that is generated as the animal moves through its environment.[1] The insect's brain rapidly processes and fuses this rich information stream to create a motor code that can modify wing motion on a stroke by stroke basis.[2] Sensory feedback is essential both for short-term stability as well as long-term guidance and navigation. What we view as behavior, such as a fly flitting across the room to land on the window, represents the output of a complex set of sensory-motor circuits that operates through the dynamics of muscles, skeleton, aerodynamics forces, and the environment. Although biologists have appreciated the central role of feedback in flight,[3] conventional biological disciplines such as neurobiology or biomechanics are not endowed with the mathematical framework to deal with the feedback in a rigorous manner. Fortunately, recent progress in insect aerodynamics has fostered new engineering approaches such as the application of control theory to animal flight.[4,5] Such work will be critical in further developing an integrative view of flight biology, if for no other reason that it will provide a rigorous framework for incorporating observations from multiple disciplines within a single context, as well as permit experiments that are not possible on a real animal. Indeed, the very nature of feedback dominated systems is that they are robust to ablation and perturbation, a fact that renders them resistant to standard reductionist methods.

In this paper we present our first attempts at constructing a 3D dynamic model of the flight system of a flying insect, the fruit fly, *Drosophila melanogaster*. Flies provide a convenient scaffold for an integrated control model, because they have been subject to extensive investigations of aerodynamics, sensory processing, and motor control.[6–22] In constructing this model, we target both short-term and long-terms goals. Immediately, we can ask if our understanding of fly aerodynamics, neurobiology, and biophysics is sufficient

*Postdoctoral Scholar, Bioengineering, California Institute of Technology.

†Esther M. and Abe M. Zarem Professor, Bioengineering, California Institute of Technology.

to create a simulated entity that can fly stably in a manner that captures some of the salient features of a real fly. Towards this end, we must be careful not to bias our conclusions by deliberately choosing free parameters that result in satisfactory performance but are not justified physiologically. The challenge here is that certain features of our model are well constrained by detailed observation and experiment and easily formulated (e.g. wing and body aerodynamics), while other components are poorly understood and may be only roughly hewed in mathematical terms (e.g. neural circuitry and wing hinge mechanics). Despite this limitation, we feel that enough is known regarding this particular organism to warrant such an attempt. The long-term goal, which is not contingent on immediate success, is to construct a model that will serve as a framework for future studies. As research on flight biology continues, black box simplifications that are currently necessary will be replaced by more rigorous "bottom up" formulation, advancing both the predictive power and physical reality of the model. The most satisfying result would be to create a useful research tool that, in conjunction with experiments on real animals, provides new insight into the underlying biology.

Our model is based on a framework that combines a simulation of insect flight dynamics, a model of insect sensory systems, and a model of the flight environment. Using this framework, control strategies can be evaluated by allowing the outputs of the sensory systems to modulate the forces produced by the wings and the results assessed in a quantitative manner. The simulation framework consists of five main components.

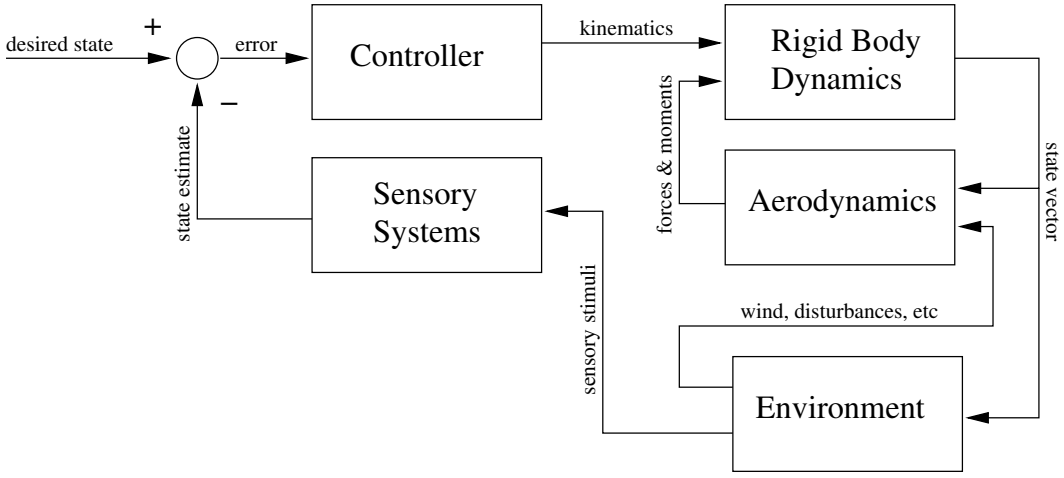

Figure 1. Block diagram illustrating the overall architecture of the simulation Framework

1. *Articulated rigid-body simulation.* A system of rigid-bodies is used to model the dynamics of the fly. A two winged insect, such as a fruit fly, is modeled as three separate rigid-bodies representing the wings and body. The wings are connected to the body with actuated ball-joints that enable the wings to track the desired kinematics. Whereas the framework has been developed using a two winged insect, it is easily modified to deal with four winged animals.

2. *Aerodynamic model.* The aerodynamic model provides estimates of the aerodynamic forces and moments during flight. The force and moment model is derived from experimental measurements obtained using a dynamically-scaled robotic model. A quasi-steady blade element model is used to estimate the forces and moments produced by the wings. The model of the forces and moments acting on the body of the fly was developed from force and moment coefficients measured using a dynamically-scaled body model in a tow tank.

3. *Sensory systems model.* As it is not currently practical to attempt to model all of the sensory systems of a fruit fly, our model focuses on the two key sensory systems that are arguably most important for flight control, the visual system and the halteres. These systems can provide information concerning the rate of change of key variables such as pitch, roll and yaw as well indicating the presence of approaching obstacles or distant targets. They thus make up the basis of both a control and navigation system. Additional components, such as an olfactory system, may be readily incorporated in the future.

4. *Control model.* The control model consists of a set of control laws specifying the behavior of the insect with regard to sensory input. The control model provides a means by which the outputs of the sensory system modulate the wing kinematics thus providing actuation. Using this framework different control strategies can be systematically evaluated and compared with the results of laboratory experiments to provide insight into insect flight control and behavior. Although the changes in wing motion generated by the control model are based on observation of real flies[20] the control model nevertheless represent the most coarsely rendered component of the model. No attempt was made, for example, to accurately model neural circuitry or musculoskeletal dynamics.

5. *Environment model.* The environment model provides input to both the sensory systems and the aerodynamics model. By providing different visual information to the sensory organs, the environment model enables us the flexibility of placing the insect in different virtual habitats, simulating both field and laboratory conditions. We can also add physical features such as wind gusts to provide realistic or arbitrary perturbations.

A schematic block diagram illustrating the interconnections between the components of the insect flight simulation framework is shown in Figure 1.

II. Simulation Framework

The simulation framework consists of four separate software components encapsulating the aerodynamics, sensory, control, and environmental models. In addition the framework provides an Application Programming Interface (API) through which the model parameters can be accessed and the interaction between the various components can specified. An overall goal is to provide a unified interface for rapidly developing insect flight mechanics and control simulations. In this section we briefly describe the models underlying the main components of the simulation framework.

A. Articulated Rigid-Body Dynamics

The dynamics of the fly are provided by an articulated rigid-body simulation. Articulated rigid-body simulation is an extension of rigid-body simulation where the bodies are attached to each other using joints.[23,24] Several different types of joints can be used to connect the bodies. Joints differ from each other in the degrees of freedom of relative motion allowed. Examples of possible joints include ball-joints, universal joints, and hinges with three, two, and one degrees of freedom respectively. In our simulation, a two winged insect such as a fly is represented by a system of three separate rigid-bodies representing the wings and body. A rendering of the articulated rigid-body system used too represent a *Drosophila* is shown in Figure 2. The

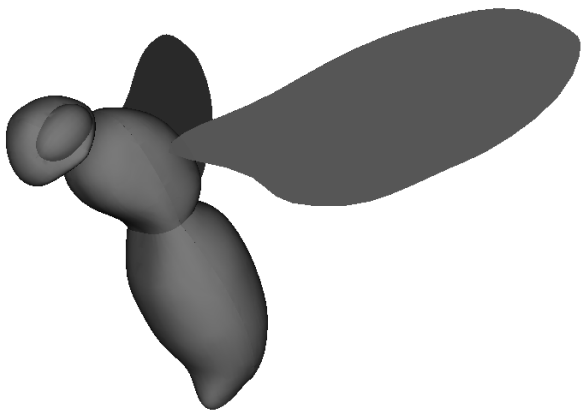

Figure 2. Rendering of the articulated rigid body-structure used to represent a *Drosophila*.

wings are connected to the body using ball-joints which are actuated to provide relative motion between the bodies in the rigid-body system. In our simulation the ball-joints representing the wing hinges are actuated by virtual angular motors to allow the wings to track the desired kinematics.

1. *Physics Engine*

At the heart of the articulated rigid-body simulation is a high performance physics library or physics engine. The physics engine provides a simulation of Newtonian physics for the rigid-body systems. For an introduction to the mathematical methods used in physics engines and articulated rigid-body dynamics the reader is referred to Ref. 23 and Ref. 24. Physics engines are commonly used in the computer gaming industry for developing interactive games as well as by the engineering community for studying manipulation and control strategies for robotic systems. For this reason there are many high quality physics engines available both commercially (Havok, Meqon, Novodex) and as open source software (Open Dynamics Engine, Dynamechs).

Several criteria were evaluated when selecting a physics engine for the project including the existence usable API, good documentation, bindings to high level languages such as Python or Ruby, an active developer community, and the availability of source code. Open Dynamics Engine (ODE) developed by Russel Smith and released under the LGPL open source license was found to be an excellent fit to these criteria.[25] ODE is a full featured industrial quality physics engine which includes many advanced joint types, integrated collision detection and a C/C++ API. Bindings to ODE are available in both Python and Ruby enabling rapid scripting using a high-level languages. In addition to several commercial computer games, ODE has been used in both biomechanics and robotics research.[26–28] The equations of motion for rigid-body systems are derived from a Lagrange multiplier velocity based model.[29]

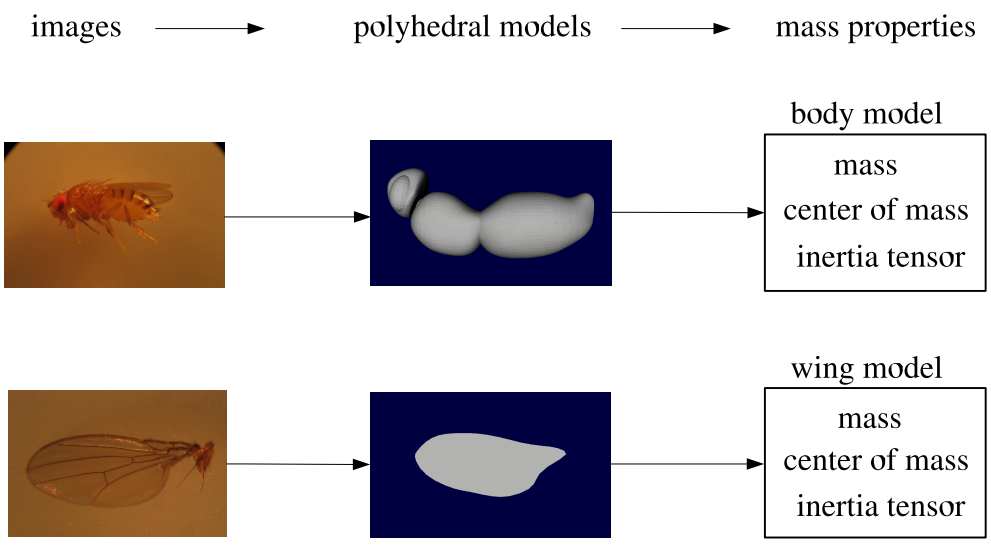

Figure 3. Schematic of procedure for generating polygonal boundary representations and determine the mass properties.

2. *Mass Properties*

In order to generate an accurate simulation of the flight dynamics of a insect it is necessary to have an accurate estimate of the mass properties of the rigid bodies used in its representation. The mass properties of a rigid body are the total mass, center of mass, and inertia tensor. Thus for our fruit fly model, based on three rigid bodies, we need to estimate the mass, center of mass and inertia tensor for each of the three bodies in the representation. In addition, to facilitate rapid changes in configuration, a systematic approach to estimating the mass properties of a given body from a polygonal boundary representation was desired.

Our basic strategy for generating polygonal models and estimating their mass properties is outlined below.

i.) Image Collection. Calibrated digital images of the object are collected from sufficient of vantage points to enable reconstruction of the object.

ii.) Boundary Model. Using the collected images a polygonal boundary representation of the object is developed with a CAD program (e.g. SolidWorks) or 3D modeling software (e.g. Blender).

iii.) Mass Properties. From the polygonal boundary representation of the object and an estimate its density the mass properties are calculated using Mirtich's algorithm.[30]

The use Mirtich's algorithm restricts this approach to objects or bodies which have uniform density. For the *Drosophila* simulation all three rigid-bodies in the representation are assumed to have a uniform density equal to that of water. This produces a mass value similar to those measured in real flies. A schematic overview of the procedure outlined above is shown in Figure 3.

B. Aerodynamic Forces and Moments

The aerodynamic model is used to calculate the forces and moments acting on the body and wings of the insect during flight. The model is quasi-steady and is based on empirically determined force and moment coefficients. The quasi-steady assumption that is based on the observation the flow pattern and forces acting on a revolving wing display little time dependence even at angles of attack high enough to generate an leading edge vortex.[18,31] The aerodynamics forces and moments generated by the wings and body are considered separately and it is assumed that they are not influenced by wing-wing and wing-body interactions.

1. Wing Aerodynamics

The wing aerodynamics model is based on prior work using a dynamically scaled physical model.[16,18,19] In this model the wing is approximated by a flat plate with planform based on a *Drosophila* wing. Using a standard blade element method, the wing is divided spanwise into a finite number of blade elements on which the forces and moments are calculated. The force on each blade element is calculated as the sum of the steady state, rotational, and added mass components

$$\mathbf{F} = \mathbf{F}_s + \mathbf{F}_r + \mathbf{F}_a. \tag{1}$$

The total force on the acting on the wing is given by the sum of the blade element forces. However, in order to generate the appropriate moments acting on the wing, the force produced by each blade element must be applied to the rigid-body representing the wing in the appropriate location. This location for a given blade element is roughly approximated by mean spanwise location of the element and the chordwise position of the center of pressure for the element. The methods used for calculating the three force components in equation (1) as well for predicting the chordwise position of the center of pressure are summarized below.

The steady state component of the force acting on a blade element is convienently expressed in terms of lift and drag. The steady state lift and drag are proportional to the product of the air density ρ, the element chord length c, the element width Δr, and the square of the incident flow velocity in the plane of the blade element, $\mathbf{u}_e$. Note, the plane of the a blade element is defined as the subspace spanned by the wing normal and wing chord vectors that intersects the center line of the element. Expressions for the magnitudes of the steady state lift and drag are given as follows

$$F_{s,\text{lift}} = \frac{1}{2}\,\rho\, c\, ||\mathbf{u}_e||^2\, C_L(\alpha)\,\Delta r \qquad \text{and} \qquad F_{s,\text{drag}} = \frac{1}{2}\,\rho\, c\, ||\mathbf{u}_e||^2\, C_D(\alpha)\,\Delta r \tag{2}$$

where α is the local angle of attack of the blade element and the lift and drag coefficients, $C_L(\alpha)$ and $C_D(\alpha)$, are shown in figure (4). The lift and drag coefficients were generated experimentally using a revolving dynamically scaled model *Drosophila* wing.[16]

The magnitude of rotational force is proportional to the product of the fluid density, the square of the element chord length, the element width, the rate of change in angle of attack $\dot{\alpha}$, and the magnitude of the incident flow velocity in the plane of the blade element. The rotational force always acts in a direction normal to the surface of the wing and an expression for its magnitude is given by

$$F_r = C_r\,\rho\,\dot{\alpha}\,c^2\;||\mathbf{u}_e||\;\Delta r \tag{3}$$

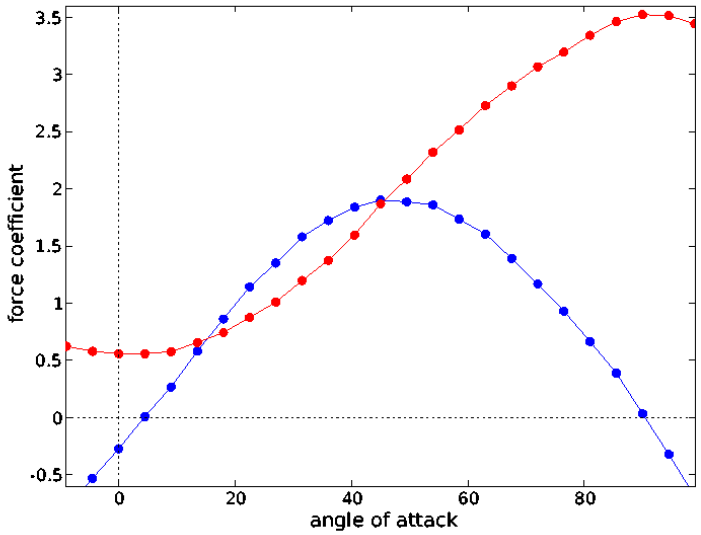

Figure 4. Steady state lift (blue) and drag (red) coefficients for revolving model *Drosophila* wing.

where C_r is the rotational force coefficient. A value of $C_r = 1.55$ is suggested by Sane in Ref. 19 as appropriate for *Drosophila* wing. This value is essentially equivalent to the value derived by Fung[32] using thin airfoil theory and assuming that rotational axis of the wing is located at 1/4 chord.

The added mass force acting on a blade element is proportional to the density of the fluid, the square of the element chord length, the element width, and the acceleration of the incident flow normal to the surface of the element. The added mass force is assumed to always act normal to the surface of the wing. An expression for the magnitude of the added mass force is given by

$$F_a = \frac{\rho \pi c^2}{4} \left\{ \frac{\mathbf{u}_e \cdot \dot{\mathbf{u}}_e}{||\mathbf{u}_e||} \sin\alpha + ||\mathbf{u}_e|| \, \dot{\alpha} \cos\alpha \right\} \Delta r \tag{4}$$

This estimate for the added mass force acting on blade element is based on an approximation for the motions of an infinitesimally thin flat plate in an inviscid fluid, for example see Sedov.[33]

Measurements using a model *Drosophila* wing demonstrate that the spanwise location of the center of pressure is approximately constant with respect changes angle of attack. This is in good agreement with predictions by the quasi-steady model as shown in Figure 5(a).

An approximately linear relationship is found between angle of attack and the chordwise location of the center of pressure as shown in Figure 5(b). This linear relationship is well approximated by the following equation

$$x_{cp}(\alpha) = c \left[0.82 \frac{|\alpha|}{\pi} + 0.05 \right]. \tag{5}$$

In order to generate the appropriate moments acting on the entire wing, the force acting on each blade element is applied at the spanwise location (or center) of the element and at the center of pressure determined by $x_{cp}(\alpha)$ where α is the local angle of attack of the element.

2. Body Aerodynamics

The body aerodynamics model is used to calculate the forces and moments acting on the body of the insect during flight. During the rigid-body simulation all the separately calculated body forces and moments are applied at the center of mass of the insect's body. The model assumes that the body of the insect is bilaterally symmetric. Under this assumption the force and moment coefficients for the body are a function of the angle of attack of the body α, the sideslip angle β, and the Reynolds number (Re). In practice, the dependence of force and moment coefficients on Re can be generally be ignored. This is due to the fact that variation

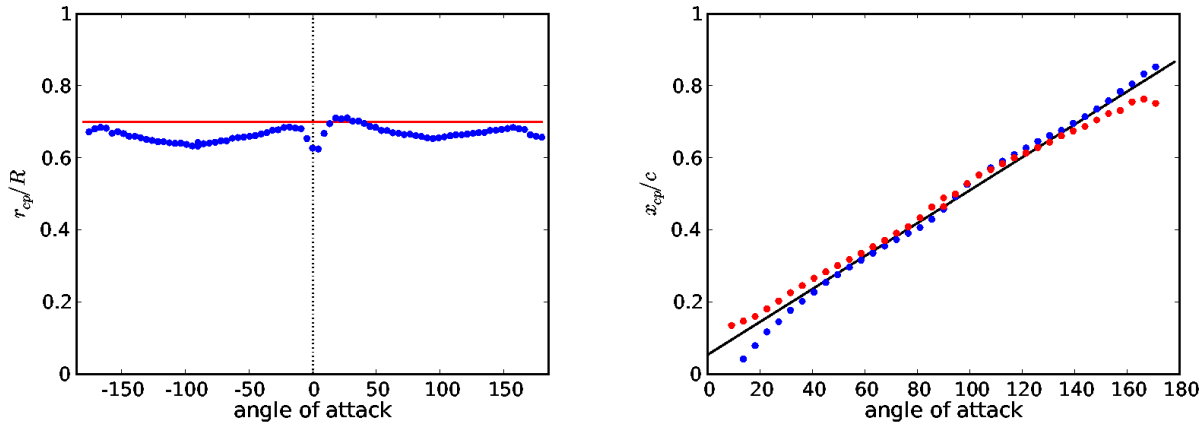

(a) (b)

Figure 5. Position of the center of pressure as a function of angle of attack. (a) Spanwise position of the center pressure (blue) blade element prediction (Red). (b) Chordwise position of the center of pressure. Positive angles of attack (blue) and negative angles of attack (red). The linear fit provided by equation (5) is shown for comparison (black)

of the coefficients with Re is only significant at very low flight speeds where the forces and moments are negligiblely small.

The forces parallel and normal to the body of the insect are proportional to the product of the fluid density, the body reference area S, and the square of the incident velocity $\mathbf{u}_b$. Expressions for the magnitudes of the parallel and normal forces are given by

$$F_P = \frac{1}{2}\,\rho\, C_P(\delta) S\, ||\mathbf{u}_b||^2 \qquad \text{and} \qquad F_N = \frac{1}{2}\,\rho\, C_N(\delta) S\, ||\mathbf{u}_b||^2 \tag{6}$$

where $C_P(\delta)$ and $C_N(\delta)$ are experimentally determined coefficients and δ is is the angle between the longitudinal body axis and the incident flow. The angle δ can be expressed in terms of the angle of attack and sideslip angle of the body as follows.

$$\delta(\alpha, \beta) = \tan^{-1}\left(\sqrt{\tan^2\alpha + \tan^2\beta}\,\right) \tag{7}$$

The normal and parallel force coefficients, $C_P(\delta)$ and $C_N(\delta)$, exhibit a simple trigonometric dependence upon the angle δ as shown in Figure 6(a). This dependence can be adequately modeled using the following expressions

$$C_P(\delta) = k_P \cos\delta \qquad \text{and} \qquad C_N(\delta) = k_N \sin\delta \tag{8}$$

where the constants k_P and k_N are determined using a linear regression. For *Drosophila* values $k_P = 0.6$ and $k_N = 1.2$ are found to be suitable. Note, the results depend upon the choice reference area, S, used when calculating the force coefficients from experimental data. For this study the reference area was selected to be that given by the projection onto the frontal plane of the body.

Moments generated during steady translation of the body about the roll axis were found to be negligiblely small compared to the moments about the pitch and yaw axes. For this reason the rolling moment produced by the aerodynamic forces acting on the body is assumed to be zero. The pitching and yawing moments are found to depend upon the density of the fluid, the length of the body L, the area of the body S, and the incident velocity $\mathbf{u}_b$. Expressions for the pitching and yawing moments are given by

$$M_P = \frac{1}{2}\,\rho\, C_{\text{pitch}}(\alpha, \beta)\, S\, L\, ||\mathbf{u}_b||^2 \qquad \text{and} \qquad M_Y = \frac{1}{2}\,\rho\, C_{\text{yaw}}(\alpha, \beta)\, S\, L\, ||\mathbf{u}_b||^2 \tag{9}$$

where $C_{\text{pitch}}(\alpha, \beta)$ and $C_{\text{yaw}}(\alpha, \beta)$ are experimentally determined pitching and yawing moment coefficients. As an example the experimentally determined pitching moment for the body as a function of angle of attack

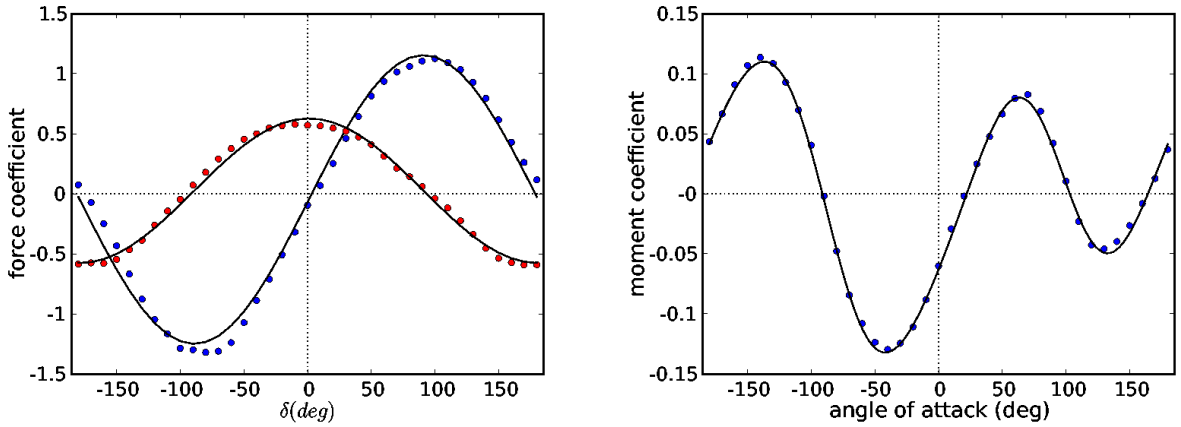

(a) (b)

Figure 6. Experimentally determined normal force, parallel force and pitching moment coefficients for the fly body. (a) Normal force coefficient (blue). Parallel force coefficient (red). A fit of the trigonometric functions (8) are shown for comparison (black). (b) Pitching moment coefficient (blue) and a fit of equation (10) for comparison (black)

is shown in Figure 6(b) for a sideslip angle of zero. The dependence of pitching and yawing moments on angle of attack and sideslip angle can be approximated using the following functions

$$C_{\text{pitch}}(\alpha,\beta) = \frac{(1+\cos 2\beta)}{2}\left\{ f(\delta(\alpha,\beta))\frac{(1+\cos\beta)}{2} + f(-\delta(\alpha,\beta))\frac{(1-\cos\beta)}{2}\right\}, \tag{10}$$

and

$$C_{\text{yaw}}(\alpha,\beta) = \frac{(1-\cos 2\beta)}{2}\left\{ f(\delta(\alpha,\beta))\frac{(1+\cos\beta)}{2} + f(-\delta(\alpha,\beta))\frac{(1-\cos\beta)}{2}\right\} \tag{11}$$

where

$$f(\delta) = \sum_{n=1}^{N} A_n \sin n\,\delta + B_n \cos n\,\delta \tag{12}$$

The values of the A_n and B_n in the function f are determined using a least squares regression to the experimentally measured pitching and yawing moments for suitable choice of N. In practice a value of $N = 4$ has been found to yield a reasonable fit.

C. Sensory Systems

1. The Visual System

To provide visually mediated signals for use in the integrated model, we sought to capture faithfully much of the known biology of the *Drosophila* visual system. The most well studied region of the fly visual system, or any visual system for that matter, is the lobula plate, which contains roughly 60 large field tangential cells sensitive to wide field motion. These large neurons spatially pool local motion information from a large region of visual space, with locally varying preferred directions.[34] Recent research suggests that many of these cells may function as matched filters for the patterns of flow that are generated by self-motion during flight.[35] Very detailed models, based on the Hassenstein-Reichardt elementary motion detector (H-R EMD)[36] have been proposed to explain the responses of neurons in this pathway and their role in flight control.[37–39] The inputs of our visual system model are driven by a 3D computer graphics engine that is a component of the environment model. From this graphics engine, an optically realistic model forms a time-varying sequence of images for processing by a simulated visual nervous system modified slightly from previous work.[40] A Mercator projection of the intensity and color of light falling on each photoreceptor in the simulated fly is

shown in Figure 7. The optical model simulates the spatial low pass filtering of each ommatidium, or facet lens, of the eye using a Gaussian filter

$$G(\zeta) = \exp\left[\frac{-4\log(2)\zeta^2}{\Delta\rho^2}\right] \tag{13}$$

where ζ is the angle from the optical axis of the ommatidium, and $\Delta\rho$ is the acceptance angle.[6] We use $\Delta\rho = k\Delta\phi$ where $\Delta\phi$ is the inter-ommatidial angle and $k = 1.1$ as found by Buchner (Ref. 41) for *Drosophila*. For the purposes of this optical lowpass filtering the inter-ommatidial angle is given by $\Delta\phi = 6.8°$, although the geometrical arrangement of optical axes actually varied in the range $6.8° - 9.3°$. Optical axes directions were constructed by sub-dividing each triangular face of a regular icosahedron into four smaller triangles. This process was repeated a total of three times, resulting in an eye with 642 ommatidia arranged nearly uniformly around the unit sphere, creating a rough approximation to the panoramic visual system of *Drosophila*.

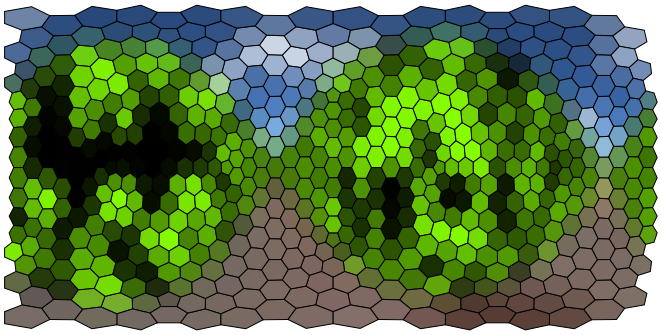

Figure 7. A Mercator projection of the intensity and color of light falling on each photoreceptor in the simulated fly. The inputs are calculated by multiplying a pre-computed weight map for each photoreceptor with the environmental cubemap to produce a physically realistic simulation of optical low pass filtering.

The first stage of neural processing is the transduction of light energy into neural signals, a process which filters out high frequency components of visual information. For each facet lens in our model, we simulated a photoreceptor with temporal dynamics given by a linear filter which closely matches the temporal dynamics of a fly photoreceptor response.[42] The impulse response of this filter is given by

$$V(t) = \exp\left[-\frac{\left(\log\frac{t}{t_p}\right)^2}{2\sigma^2}\right] \tag{14}$$

where t_p is the time to peak and σ specifies the width. For the simulations presented here $t_p = 15$ms and $\sigma = 0.32$, although these faster than responses measured in *Drosophila*.

The following stages of visual modeling are modeled as an H-R EMD. Although more elaborate correlator models have been proposed we have chosen to use a simpler implementation. Consider the time-varying output of two photoreceptors $V_A(t)$ and $V_B(t)$. Such a signal, when filtered with a linear, first-order lowpass filter, will be delayed and is denoted $V'_A(t)$ or $V'_B(t)$. Thus $V'_A(t)\,V_B(t)$ is the product of the temporally delayed photoreceptor output $V'_A(t)$ with the undelayed output $V_B(t)$. Our delay filter is of the form

$$f_\tau(t) = \frac{1}{\tau}\exp\left(-\frac{t}{\tau}\right) \tag{15}$$

where the time constant τ is set to 35 msec. The output of an EMD is defined to be two such mirror-symmetric subunits subtracted

$$V_{\mathrm{EMD}}(t) = V'_A(t)\,V_B(t) - V_A(t)\,V'_B(t). \tag{16}$$

On our eye of 642 photoreceptors, there are 1940 possible EMDs when taking adjacent inputs. For our present model, we selected the 500 EMDs most sensitive to horizontal motion and averaged them such that

we had a single, wide-field motion sensitive neuron. We foresee implementing a more realistic network of similar neurons in future models. We confirmed that the outputs of this neuron generate a strong output signal upon rotation and that the sign reversed when rotating in the opposite direction. Further the response is near zero when there is equal and opposite optic flow on the two sides of the eye such as during forward translation in the middle of a tunnel. Although flies have roughly 60 wide field cells in the lobula plate, our present model incorporates only this single element.

2. The Halteres

In Diptera, including fruit flies, the pair of hindwings are modified into pair of dumb-bell shaped shape organs with a knob-like end and a stiff stalk. These organs are called halteres play an import role in flight stabilization. It has long been known that flies are unable to fly when their halteres are removed or immobilized.[43] During flight the halteres oscillate in antiphase with the wings in planes that are tilted back from the sagital plane by approximately 30°. The stalk of the haltere is heavily innervated with approximately 400 mechanoreceptors.[44–46] A subset of these mechanorecptors transduce information concerning the rotational velocity of the fly because they are exclusively sensitive the lateral deflections of the haltere within its stroke plane. Lateral forces are not caused by the back and forth beating of the haltere, but are generated by Coriolis forces caused by the angular rotation of the fly.[47] An expression for the Coriolis force acting the haltere of a fly during flight is given by

$$F = -2m\,(\omega \times v) \tag{17}$$

where m is the mass of the haltere end knob, ω is the angular velocity of the fly, and v is the velocity of the end knob of the haltere relative to the fly.[47] Note, a subscript L or R will be used when referring specifically to left or right haltere respectively.

The haltere model assumes that the mass of the haltere is located in the end knob which is approximated as a point mass. The angular position of the haltere within the stroke plane is given by the periodic function $\psi(t)$ which is antiphase with the wing stroke position. The velocity of the left and right haltere end knobs relative to the fly are given by

$$\mathbf{v}_L(t) = \Big[\quad \dot{\psi}(t)\, d\cos\theta\sin\psi(t),\quad \dot{\psi}(t)\, d\cos\psi(t),\quad \dot{\psi}(t)\, d\sin\theta\sin\psi(t)\Big]^T \tag{18}$$

and

$$\mathbf{v}_R(t) = \Big[-\dot{\psi}(t)\, d\cos\theta\sin\psi(t),\quad \dot{\psi}(t)\, d\cos\psi(t),\quad \dot{\psi}(t)\, d\sin\theta\sin\psi(t)\Big]^T \tag{19}$$

respectively, where d is the length of the haltere and θ is the angle between the haltere stroke plane and the sagital plane. In this description the pitch, yaw, and roll axes of the fly are given by the x, y, and z body axes respectively. The lateral components of the Coriolis forces acting on the left and right halters halteres are then given by

$$F_L(t) = -2\,m\,\dot{\psi}(t)\,d\,\left[\,\omega_x(t)\cos\theta\cos\psi(t) - \omega_y(t)\sin\psi(t) + \omega_z(t)\sin\theta\cos\psi(t)\right] \tag{20}$$

and

$$F_R(t) = -2\,m\,\dot{\psi}(t)\,d\,\left[\,\omega_x(t)\cos\theta\cos\psi(t) + \omega_y(t)\sin\psi(t) - \omega_z(t)\sin\theta\cos\psi(t)\right] \tag{21}$$

respectively where ω_x, ω_y and ω_z are the x, y and z components of the angular velocity vector. From equations (20) and (21) it is apparent that the Coriolis force acting on the haltere is complex waveform whose value at any given instant depends upon the velocity of the haltere, the stoke position of the haltere, and the three components of the angular velocity vector.

A region of the haltere stalk, called the basal plate, contains numerous fields of companiform sensilla near the base of the haltere. One field in particular (dF2) is known to be particularly sensitive to lateral deflection and is thought to act as the Coriolis detector.[48] In this manner the fly is able to sense the lateral component of the Coriolis forces. The neural processing of these signals is poorly understood. However, it is thought that flies can sense all three components of the angular velocity vector using both of their halteres.[49,50] In order to use the halteres for sensory feedback in our integrated flight control model a scheme for converting the forces sensed by the halteres into changes in wing kinematics is required. As the neural processing by which this is done in the fruit fly is in general not well understood it is necessary for us posit a plausible scheme instead. A first step in such a scheme is an estimate of the angular velocity from the Coriolis forces

or resulting strains. Below we outline a method for extracting the three components of the angular velocity vector using the lateral components of the Coriolis force from both halteres. While this method can not be viewed as an accurate model of sensory processing in the fly it does provide a method which is at least theoretically possible given the sensory information available.

Examining equations (20) and (21) it is apparent that by adding the lateral components of the Coriolis forces of the left and right halteres the roll ω_z and yaw ω_y components of the angular velocity cancel. Thus we can solve for the pitch rate ω_x as follows

$$\omega_x(t) = -\frac{F_L(t) + F_R(t)}{4\, m\, d\, \dot{\psi}(t) \cos\theta \cos\psi(t)}. \tag{22}$$

The denominator in equation (22) is equal to zero only at stroke reversals when $\dot{\phi}(t)$ is equal to zero and at mid-halfstroke when $\cos\phi(t)$ is equal to zero.

Subtracting the lateral components of the Coriolis forces of the left and right halteres, equations (20) and (21), yields an expression containing only the roll ω_z and yaw ω_y rates

$$F_L(t) - F_R(t) = 4\, m\, \dot{\psi}(t)\, d\, \left[\omega_y(t) \sin\psi(t) - \omega_z(t) \sin\theta \cos\psi(t)\right]. \tag{23}$$

The roll and yaw rates, $\omega_y(t)$ and $\omega_z(t)$, can be estimated from equation (23) using a series of lagged measurements from a window of length δt. The measurement window is divided into $N+1$ time points

$$t_i = t - \frac{i\delta t}{N} \tag{24}$$

where $i = 0, \ldots, N$. In the measurement window the roll and yaw rates are approximated by the k-th order polynomials

$$\omega_y(t) \approx \sum_{i=0}^{k} a_i t^i \tag{25}$$

and

$$\omega_z(t) \approx \sum_{i=0}^{k} b_i t^i. \tag{26}$$

Inserting equations (25) and (26) into equation (23) for $t = t_0, \ldots t_N$ yields a set of $N+1$ linear equations with $2(k+1)$ unknowns which can be solved for the unknowns a_i and b_i. The estimate for the roll and yaw rates a time $t = t_0$ is then given by $\omega_y(t_0)$ and $\omega_z(t_0)$ respectively. Values of $k = 1$ and $N = 20$ have been found to good results.

Temporal aspects of the neural processing of haltere sensory information are approximated with a filter based on observations of the haltere mediated responses of *Drosophila*.[51] The transfer function of the filter is given by

$$G(s) = \frac{1.873s + 10.08}{s^2 + 20.5s + 134.3}. \tag{27}$$

which has complex poles at $-10.26 \pm 5.41i$ and is based on a fit to experimental data.[51] This filter is applied to the roll, pitch and yaw rates estimated from the lateral components of the Coriolis forces.

D. Environment Model

The environment model is used to represent the environment external to the insect. It provides inputs to both the sensory models (visual, mechanosensory) and the aerodynamics models (wind, gusts). Currently, the environment model consists of two main components. A 3D graphics engine which generates optically realistic images for processing by the visual system and a wind/gust model to provide steady and transient perturbations to the insect during flight.

1. Visual Environment + 3D Graphics Engine

A computer model of three dimensional terrain and other objects provides input to the simulated visual system. The model is constructed using a program that generates arbitrary primitives, such as a textured ground surface or a wall with a checkered pattern. Such virtual objects are loaded into the rendering

engine, which is built using Open Scene Graph, a free, open source library for displaying realistic scenes in realtime for computer games and visual simulations Figure 8(a). At each sampling instant, the rendering engine produces six images such that a cube of snapshots is formed around the simulated fly's position and orientation. This "cubemap", shown in Figure 8(b), represents the color and luminance of the environment in any direction from the observer's perspective. From this information, the intensity of light falling on each simulated photoreceptor is calculated by the visual system model.

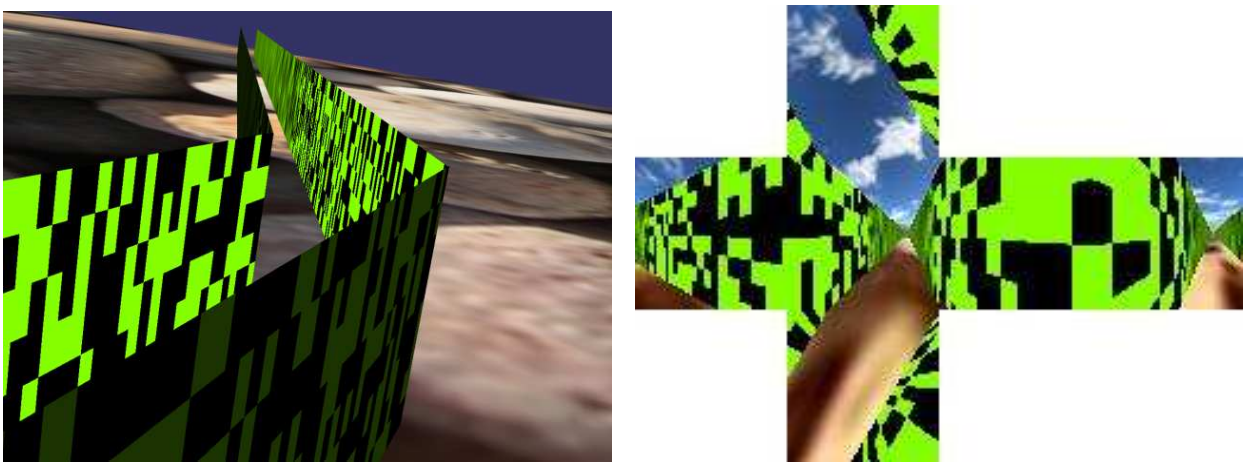

(a) (b)

Figure 8. (a) A view of the simulated 3D environment within the Open Scene Graph engine. (b) A cubemap representing the visible environment from the position and orientation of the simulated fly's head.

2. Wind and Gusts

The wind and gust models enable us to apply either a steady wind or various transient gusts to perturb the flight of the insect. The ability to apply steady wind effectively enables us to decouple the ground-speed and airspeed. As many of the proposed flight control strategies for insects rely on feedback from the visual system, effectively measuring ground speed,[52] this decoupling is crucial in order to analyze their performance. The gust model enables the user to apply transient perturbations to an insect as it flies. Using the gust model, the stability and robustness of various control strategies can be accessed. Gusts can be either temporal or spatial and may be applied to any combination of axes. For example, a temporal step gust in the can specified as follows

$$\mathbf{V}(t) = \begin{cases} \mathbf{O} & \text{if} \quad t < t_g, \\ \mathbf{V}_g & \text{otherwise} \end{cases} \tag{28}$$

where $\mathbf{V}_g$ is the gust velocity vector and t_g is time at which the gust occurs. For discrete gusts the velocity transition can be a step (as above) or gradual using the standard 1-cosine model and specifying the gust length. Temporal gusts may also be sinusoidal; specified along a given direction with a given frequency and amplitude. Spatial gusts enable the user model the effects of transitioning from still air into a moving air stream. As with temporal gusts a spatial gust may be abrupt or gradual.

E. Flight Control Model

The flight control model specifies the baseline wing kinematics and a set of deformation modes that can be used to modify or deform the baseline kinematics in order to alter the aerodynamic forces produced. In addition, the flight control model specifies a set of actions or control laws by which sensory input modifies the baseline kinematics along the deformation modes. The different deformation modes represent degrees of freedom with respect to actuation, whereas the control laws specify how much deformation to apply along the given modes.

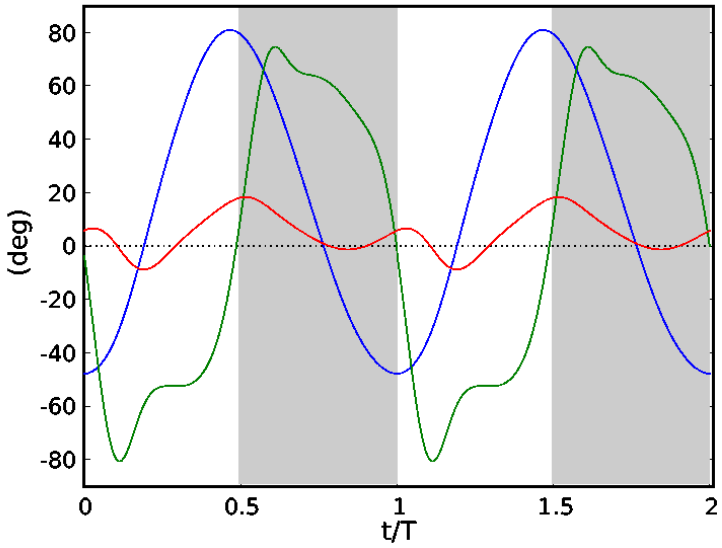

Figure 9. Baseline wing kinematics digitized from a free flying *Drosophila*. Stroke position angle ϕ (blue), stroke deviation angle θ (red), and rotation angle α (green).

1. Baseline Wing Kinematics and Deformation Modes

The angular motors controlling the motion of the wings are set up to allow essentially arbitrary wing kinematics by specifying the desired angular velocity of the wing about the wing hinge at each instant of the simulation. In this way the simulated fly is capable of utilizing both artificial and natural (digitized from high-speed video) wing kinematics. For each wing the kinematics are described by four angles, the stroke position angle ϕ, the deviation angle θ, and the rotation angle α as described in Ref. 53. The stroke position angle, ϕ, is the given by the angular position of the projection of the wing axis in the stroke plane. The deviation angle, θ is given by the angle between the stroke plane and the wing axis, and the rotation angle is given by the angular rotation of the wing about its axis. Normally, kinematics digitized from high-speed video sequences of free flying insects are used to create baseline wing kinematics for simulations.[20] Figure 9 shows a typical example of baseline wing kinematics used our simulations.

The wing deformation modes enable actuation - the modification of the aerodynamic forces by a controller. Although greatly simplified, the deformation modes are meant to roughly approximate what is known with regard to how flies modify their wing kinematics to stabilize flight and maneuver. Four different deformation modes are defined, pitch mode, yaw mode, role mode, and throttle mode. As suggested by their names the pitch, yaw and roll modes modulate the torque produced about the pitch, yaw, and roll axes respectively, whereas the throttle mode modulates the overall aerodynamic force produced by the wings. The changes in wing kinematics effected by the four deformation modes are described briefly below.

i.) Pitch mode. The pitch mode deformation modulates the torque about the pitch axis of the fly by moving the mean stroke position of the wings forward and backward. For example, to produce a forward pitch torque the mean stroke positions of the wings are moved rearward. A controller which modifies the pitch torque based on sensory input sends the desired mean stroke position angle $\langle\phi\rangle$ to the pitch mode deformation mechanism.

ii.) Yaw mode. The yaw mode deformation modulates the torque about the yaw axis of the fly by differentially adjusting the stroke amplitudes of the wings. For example, to produce a yaw torque to the left the amplitude of the right wing is increased and the amplitude of the left wing decreased. A controller which modifies yaw torque sends the desired difference between left and right wing stroke amplitudes $\Delta\phi_{LR}$ to the yaw mode deformation mechanism.

iii.) Roll mode. The roll mode deformation modulates torque about the roll axis of the fly by differentially inclining the stroke planes of the wings. For example, to produce a roll torque to the left the stroke

plane of the right wing is inclined forward and stroke plane of the left wing is inclined rearward. A controller which modifies the roll torque sends the desired difference in stoke plane inclination $\Delta\eta$ to the roll mode deformation mechanism.

iv.) Throttle mode. The throttle mode deformation modulates the overall aerodynamic force produced by the wings by adjusting the wing beat frequency and stroke amplitude of both wings simultaneously. A controller that modifies the overall aerodynamic forces sends the desired change (from the baseline kinematics) in wing beat frequency Δf and stroke amplitude $\Delta\phi$ to the throttle mode deformation mechanism.

2. Angular Velocity Control

It is known that flies control angular velocity in compensatory manner, counter steering in response visual and mechanical stimulation.[54] A basic control strategy developed for our framework emulates this by controlling the angular velocity of the fly via a simple set of proportional controllers acting directly on the pitch, yaw and roll deformation modes. Suppose the desired or set-point angular velocity vector is given by

$$\omega^* = (\omega_x^*, \omega_y^*, \omega_z^*)^T. \tag{29}$$

In order to control the pitch rate, the input to the pitch mode deformation mechanism is set to value proportional to the difference between the set-point pitch rate ω_x^* and the pitch rate as estimated from the halteres ω_x as follows

$$\langle\phi\rangle = G_p\left(\omega_x^* - \omega_x\right) \tag{30}$$

where G_p is the gain of the controller. The difference in the set-point and estimated pitch rates is referred to as the pitch rate error. In a similar fashion the inputs to the yaw and roll deformation mechanisms are set to values proportional to the yaw rate and roll rate errors respectively

$$\Delta\phi_{LR} = G_y\left(\omega_y^* - \omega_y\right) \qquad \text{and} \qquad \Delta\eta = G_r\left(\omega_z^* - \omega_z\right) \tag{31}$$

where G_y, and G_r are the gains of the controllers. This simple strategy produces a compensatory angular velocity control similar to that seen in experiments[54] when given set-point angular velocity where the pitch, yaw and roll rates are all equal to zero. In addition, by setting the angular velocity set-point to a nonzero or time varying value, simple flight maneuvers can be effected. Figure 10 demonstrates tracking of a sinusoidally varying pitch rate command by this simple controller. The oscillations in pitch rate, seen in the figure, are due to the time varying forces and torques produced by the flapping wings rather than instability in the controller.

3. Rate Based Velocity Control

Forward flight velocity in flies in known to be strongly correlated with the pitch angle of the body which suggests that forward velocity may be controlled by adjusting pitch or pitch rate.[52] One control scheme being tested using our framework employs this idea to control forward velocity using pitch rate. This is achieved by adjusting the pitch rate set-point of the angular velocity controller using the error between the desired forward velocity v_f^* and the perceived forward velocity v_f as follows

$$\omega_x^* = G_{f,0}\left(v_f^* - v_f\right) + G_{f,1}\left(\dot{v}_f^* - \dot{v}_f\right) \tag{32}$$

where the constants $G_{f,0}$ and $G_{f,1}$ are the controller gains. The first term in (32) is proportional to the velocity error and the second is proportional to the derivative of the velocity error. The derivative term has been found necessary to damp a stable limit cycle oscillation which occurs if only the proportional term is used. For a suitable choice of gains this controller has been found to yield stable forward flight at the desired velocity. In addition it provides pitch stability, effectively eliminating the slow drift in pitch that occurs when only pitch rate control is used. The response of this controller to a step input in forward velocity is shown in Figure 11. In response to the step input the fly, initially at rest, pitches forward and accelerates. It gains forward velocity and, as it approaches the set-point velocity, pitches back eventually reaching a stable pitch angle. The final pitch angle depends upon the set-point velocity in a manner similar to that found in experiments with flies in a wind tunnel.[52] Using an analogous controller the lateral velocity of the fly can also be controlled by setting the yaw rate set-point using the error between the desired lateral velocity and the perceived lateral velocity. Combining, these two control schemes gives a method by which the simulated fly can perform simple maneuvers.

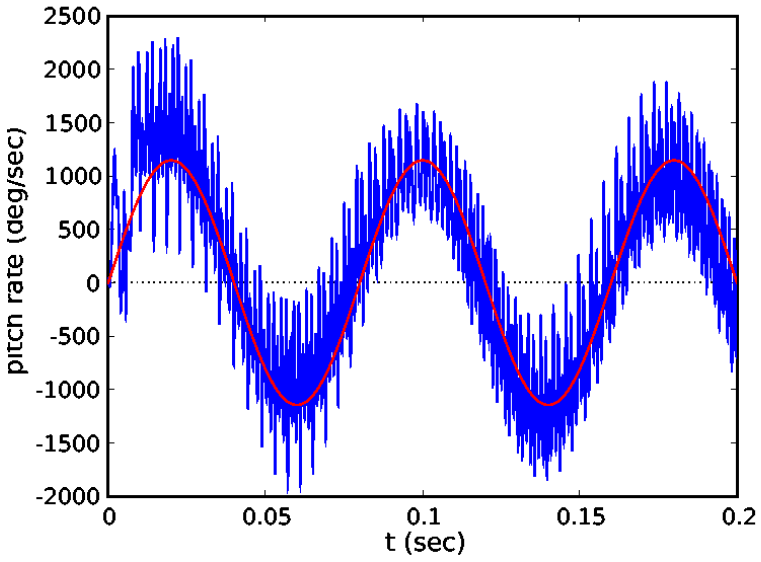

Figure 10. Example demonstrating tracking of a sinusoidally varying pitch rate command using angular velocity control. Actual pitch rate (blue), pitch rate command (red). High frequency oscillations are due to the periodic forces produced by the fly's wings and not instability in the controller.

4. Altitude Control

While the strategies used by flies control altitude and are not well understood at this time, it is useful when performing long simulations to have control schemes on hand which can be used to maintain or control the altitude of the simulated fly. Similarly, when considering issues of flight performance being able to control the rate of climb or descent is also of value. For this reason we have designed two altitude controllers which can be used during simulations.

The first is a vertical velocity controller which uses the error between the desired vertical velocity v_z^* and the estimated vertical velocity v_z to adjust the wing beat frequency and stroke amplitude of the wings using the throttle deformation modes via a simple proportional-integral control scheme

$$\Delta f = G_{f,0}\left(v_z^* - v_z\right) + G_{f,1}\int_0^t \left(v_z^* - v_z\right) \mathrm{d}s \tag{33}$$

and

$$\Delta \phi = G_{\phi,0}\left(v_z^* - v_z\right) + G_{\phi,1}\int_0^t \left(v_z^* - v_z\right) \mathrm{d}s \tag{34}$$

where $G_{f,0}$, $G_{f,1}$, $G_{\phi,0}$, and $G_{\phi,1}$ are controller gains. The values of Δf and $\Delta \phi$ are clamped to keep the wing beat frequency and stroke amplitude of the fly within a physically reasonable range. The roll of the integral terms in equations (33) and (34) is remove the steady state error which occurs when only the proportional terms are present.

The second is an altitude controller which uses the error between the desired altitude z^* and the estimated altitude z to adjust the wing beat frequency and stroke amplitude using a proportional-derivative control scheme

$$\Delta f = G_{f,0}\left(z^* - z\right) + G_{f,1}\left(\dot{z}^* - \dot{z}\right) \tag{35}$$

and

$$\Delta \phi = G_{\phi,0}\left(z^* - z\right) + G_{\phi,1}\left(\dot{z}^* - \dot{z}\right) \tag{36}$$

where again $G_{f,0}$, $G_{f,1}$, $G_{\phi,0}$, and $G_{\phi,1}$ are controller gains and the values of Δf and $\Delta \phi$ are clamped. The derivative terms in equations (35) and (36) provide damping and reduce oscillations in altitude about the set-point. Note, the control gains in equations (35) and (36) are not the same as those in equations (33) and (34) and different values are used. An example of the response of the fly to a step input when using the vertical velocity controller, equation (33), is shown in Figure 12.

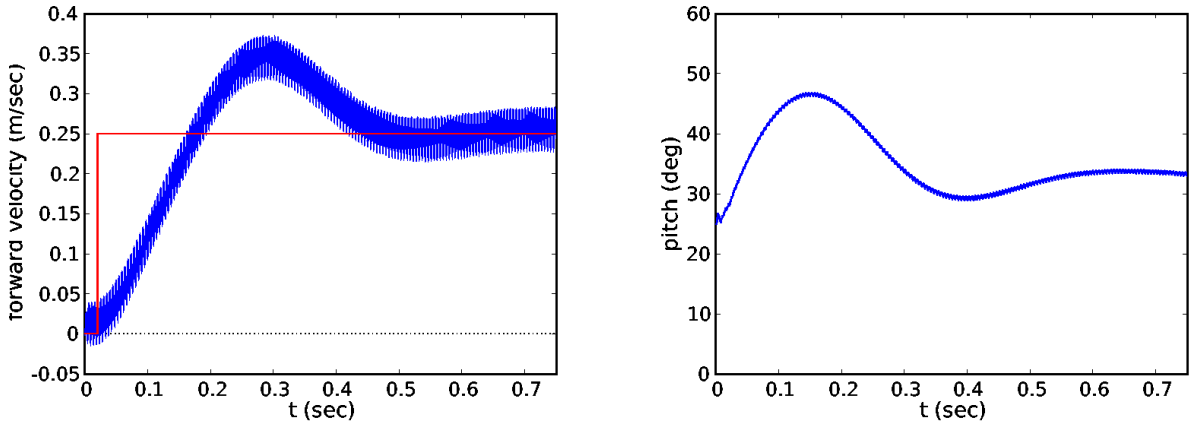

(a) (b)

Figure 11. Example of the response of the fly to step input when using the pitch rate based velocity controller. (a) Forward velocity (blue) and step input (red). (b) Pitch angle of the body (blue). High frequency oscillations are due to the periodic forces produced by the fly's wings and not instability in the controller.

5. Closed loop, visually based flight within a tunnel

A visually based upwind flight controller for tunnel geometry was developed as a preliminary demonstration of simulating more sophisticated flight behaviors. This controller was tested in a simulated tunnel environment similar to that shown in Figure 8. The basic idea behind this controller follows from the work of Humbert (Ref. 55), who investigated the output of various schemes of wide-field integration of idealized local velocity detectors not subject to the non-linear behavior of H-R EMDs discussed above. He showed that, when linearized about a mid-tunnel trajectory, a wide-field integrator that sums the magnitudes of horizontal velocities measured around the equator produces the response

$$V_{\mathrm{WFI}}(t) = -2\sqrt{2}\omega_y + 4\frac{v}{\sqrt{2}a^2}p \tag{37}$$

where p is the lateral position of the fly with respect to mid-tunnel, v is forward velocity, and a is the width of the tunnel. For small yaw rates and constant flight velocity the output wide-field integrator is approximately proportional to the lateral position of the fly with respect to mid-tunnel p. Under these conditions the output of the wide-field integrator can be used to produce a counter steering control strategy which turns right when the fly has deviated from mid-tunnel to the left and turns left when deviated from mid-tunnel to the right. This is done by setting the yaw rate set-point of the angular velocity controller to a value proportional to the output of the wide-field integrator

$$\omega_y^* = G_{\mathrm{WFI}}\ V_{\mathrm{WFI}}(t) \tag{38}$$

where G_{WFI} is a gain term and V_{WFI} is taken to be the output of our lobula plate simulation, rather than a signal derived from ideal velocity estimates. This signal provides simulated a fly, which has deviated from the tunnel mid-line, with a tendency to turn back toward the mid-line.

In order to prevent overcompensating, i.e., turning too far prior to encountering the tunnel mid-line, the control law given by equation (38) was modified so that the yaw rate set-point changed sign when the the angle between the direction of travel and the tunnel mid-line σ became larger then a given threshold. This had the additional benefit of keeping of the position within a range where the linearization of (38) remained valid. For visually estimating the angle σ, we used a blue-sensitive overhead stripe orientation detector, which was able to determine the angle of the model fly relative to the tunnel. Although there is no evidence for such a system in flies, both the polarization-sensitive dorsal rim area of the compound eyes[56] and the stripe-fixation visual circuitry[57] could be imagined to perform a similar role. Nevertheless, we emphasize this is a demonstration of feasibility of an integrated model, rather than a highly accurate biological simulation.

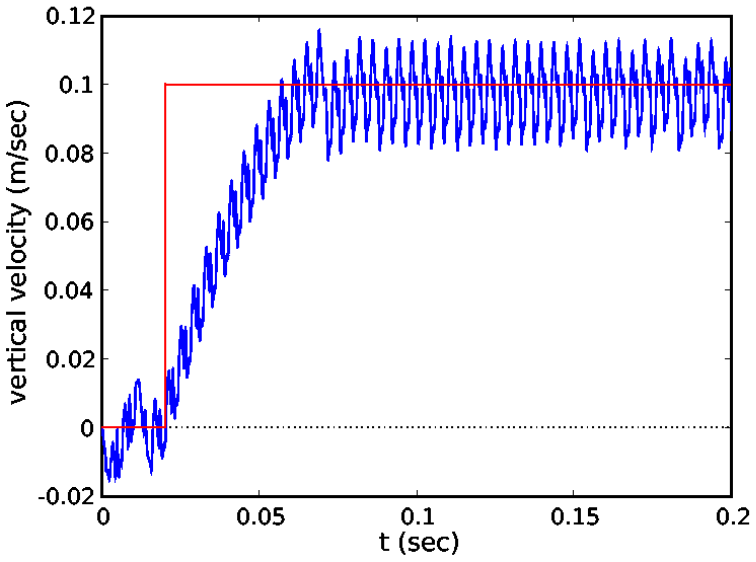

Figure 12. Example demonstrating the response of the fly to a step input when using the vertical velocity controller. Actual vertical velocity of the fly (blue), step input (red). High frequency oscillations are due to the periodic forces produced by the fly's wings and not instability in the controller.

When simulated in our environment, visually derived estimates of σ and y correspond well with the actual values, as seen in Figure 13. By using these estimates to set the yaw rate of the fly, modifying the wing kinematics based on the deformation modes described above, we closed the visual-motor feedback loop within our integrated model. The simulated fly was able to fly up the tunnel while successfully avoiding the walls. Future work will seek to investigate the robustness of such behavior with respect to environmental geometry changes and to introduce full sensory-motor control over a greater number of biologically relevant degrees of freedom such as forward velocity, altitude, and attitude in addition to heading.

III. Conclusions

In this paper, we have shown presented an integrated framework for simulating the flight dynamics and control strategies of the fruit fly. By taking a bottom-up approach based on physically and biologically realistic components, we are able to formulate and test explicit hypotheses regarding flight control at levels ranging from stroke-by-stroke stabilization of pitch to long-range flight through a tunnel. Special emphasis is placed on the sensory feedback components of the model, which limit the potential information available to controllers in our model, just as real sensory systems must do in real flies. The availability of the modeling environment enables inquiry and analysis into the principles underlying insect flight control in a closed-loop, feedback driven system. This approach is necessary due to tight coupling between motor output and multi-modal sensory input, making flight control difficult to study with traditional reductionist approaches that elucidate feed-forward mechanisms. By adopting this integrative modeling approach in conjunction with further biological experimentation, we hope we will be able to provide some insight into the nature of the solutions that endow flies with their remarkable flight and goal directed behaviors. Such an endeavor seems worthwhile, because, as anyone who has tried to rid a kitchen of fruit flies knows, these animals are robust performers in a wide range of environments and in the face of severe environmental perturbations.

Acknowledgments

This work was supported by grants from the Packard Foundation, AFOSR (F49620-03-1-0171), NSF (IBN-0217229), and ARO (DAAD 19-03-D-0004).

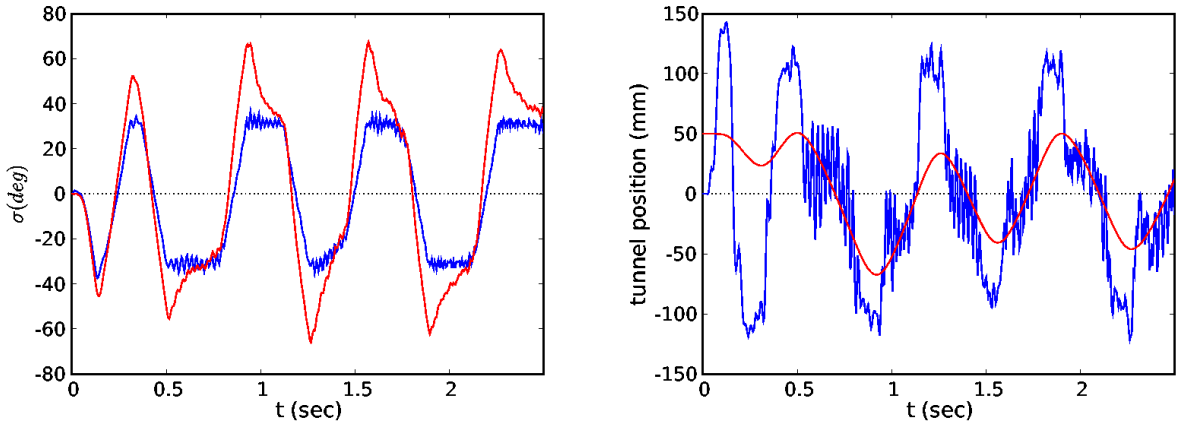

(a) (b)

Figure 13. Visually derived estimates of the σ and p. (a) Visual estimate of the angle σ (blue) and actual value (red). (b) Visual estimate of tunnel position p (blue) and actual (red).

References

[1]Strausfeld, N., *Atlas of an insect brain*, Springer-Verlag, New York, 1976.

[2]Dickinson, M., "The initiation and control of rapid flight maneuvers in fruit flies," *Integrative and Comparative Biology*, Vol. 45, No. 2, 2005, pp. 274–281.

[3]Dickinson, M., Farley, C., Full, R., Koehl, M., Kram, R., and S., L., "How animals move: An integrative view," *Science*, Vol. 288, No. 5463, 2000, pp. 100–106.

[4]Taylor, G., "Mechanics and aerodynamics of insect flight control," *Biological Reviews*, Vol. 76, No. 4, 2001, pp. 449–471.

[5]Reiser, M., Humbert, S., Dunlop, M., Vecchio, D., Murray, M., and Dickinson, M., "Vision as a compensatory mechanism for disturbance rejection in upwind flight," *American Control Conference, 2004. Proceedings of the 2004*, IEEE Computer Society, 2003, pp. 311–316.

[6]Snyder, A., "Physics of vision in compound eyes," *Handbook of Sensory Physiology*, edited by H. Autrum, Vol. VII, Springer-Verlag, Berlin, 1979, pp. 255–313.

[7]Ellington, C., "The aerodynamics of hovering insect flight. I. Lift and power requirements." *Phil. Trans. R. Soc. Lond. B*, Vol. 305, 1984, pp. 1–15.

[8]Ellington, C., "The aerodynamics of hovering insect flight. II. Morphological parameters." *Phil. Trans. R. Soc. Lond. B*, Vol. 305, 1984, pp. 17–40.

[9]Ellington, C., "The aerodynamics of hovering insect flight. III. Kinematics." *Phil. Trans. R. Soc. Lond. B*, Vol. 305, 1984, pp. 41–78.

[10]Ellington, C., "The aerodynamics of hovering insect flight. IV. Aerodynamic mechanisms." *Phil. Trans. R. Soc. Lond. B*, Vol. 305, 1984, pp. 79–115.

[11]Ellington, C., "The aerodynamics of hovering insect flight. V. A vortex theory." *Phil. Trans. R. Soc. Lond. B*, Vol. 305, 1984, pp. 115–144.

[12]Ellington, C., "The aerodynamics of hovering insect flight. VI. Lift and power requirements." *Phil. Trans. R. Soc. Lond. B*, Vol. 305, 1984, pp. 145–181.

[13]Borst, A. and Egelhaaf, M., "Principles of visual motion detection," *Trends in Neuroscience*, Vol. 12, 1989, pp. 297–306.

[14]Dickinson, M. and Gotz, K., "Unsteady aerodynamic performance of model wings at low Reynolds-numbers," *Journal of Experimental Biology*, Vol. 174, 1993, pp. 45–64.

[15]Dickinson, M., "The effects of wing rotation on unsteady aerodynamic performance at low Reynolds-numbers," *Journal of Experimental Biology*, Vol. 192, 1994, pp. 179–206.

[16]Dickinson, M., Lehmann, F., and Sane, S., "Wing rotation and the aerodynamic basis of insect flight," *Science*, Vol. 284, No. 5422, 1999, pp. 1954–1960.

[17]Birch, J. and Dickinson, M., "The influence of wing-wake interactions on the production of aerodynamic forces in flapping flight." *Journal of Experimental Biology*, Vol. 206, 2003, pp. 2257–2272.

[18]Sane, S. and Dickinson, M., "The control of flight force by a flapping wing: Lift and drag production," *Journal of Experimental Biology*, Vol. 204, No. 15, 2001, pp. 2607–2626.

[19]Sane, S. and Dickinson, M., "The aerodynamic effects of wing rotation and a revised quasi-steady model of flapping flight," *Journal of Experimental Biology*, Vol. 205, No. 8, 2002, pp. 1087–1096.

[20]Fry, S., Sayaman, R., and Dickinson, M., "The aerodynamics of free-flight maneuvers in Drosophila," *Science*, Vol. 300, No. 5618, 2003, pp. 495–498.

[21]Birch, J., Dickson, W., and Dicksinson, M., "Force production and flow structure of the leading edge vortex on flapping wings at high and low Reynolds numbers." *Journal of Experimental Biology*, Vol. 207, 2004, pp. 1063–1072.

[22]Dudley, R., *The Biomechanics of Insect Flight*, Princeton University Press, Princeton, New Jersey, 2000.

[23]Shabana, A., *Computational Dynamics*, John Wiley and Sons Inc., New York, 2001.

[24]Coutinho, M., *Dynamic Simulations of Multibody Systems*, Springer-Verlag, New York, 2001.

[25]"http://www.ode.org/," .

[26]Durikovic, R. and Numata, K., "Human hand model based on rigid body dynamics," *IV '04: Proceedings of the Information Visualisation, Eighth International Conference on (IV'04)*, IEEE Computer Society, Washington, DC, USA, 2004, pp. 853–857.

[27]Pollard, N. and Zordon, V., "Physically based grasping and control from example," *ACM SIGGRAPH / Eurographics Symposium on Computer Animation 2005*, Association for Computing Machinary, Inc., New York, 2005, pp. 311–358.

[28]Go, J., Browning, B., and Veloso, M., "Accurate and flexible simulation for dynamic, vision centric robots," *Autonomous Agents and Multiagent Systems (AAMAS 2004)*, IEEE Computer Society, New York, 2004, pp. 1386–1387.

[29]Stewart, D. and Trinkle, J., "An implicit time-stepping scheme for rigid body dynamics with inelastic collisions and Coulomb friction," *International J. Numer. Methods Engineering*, Vol. 39, 1996, pp. 2673–2691.

[30]Mirtich, B., "fast and accurate computation of polyhedral mass properties," *Journal of Graphics Tools*, Vol. 1, No. 2, 1996.

[31]Birch, J. and Dickinson, M., "Spanwise flow and the attachment of the leading- edge vortex on insect wings." *Nature*, Vol. 412, No. 6848, 2001, pp. 729–733.

[32]Fung, Y., *An Introduction to the Theory of Aeroelasticity*, New York: Dover, 1969.

[33]Sedov, L., *Two-Dimensional Problems in Hydrodynamics and Aerodynamics*, Interscience Publishers, New York, 1965.

[34]Hausen, K., "The lobula complex of the fly: Structure, function and significance in visual behavior," *Photoreception and Vision in Invertebrates*, edited by M. Ali, Plenum Press., New York, 1984, pp. 523–559.

[35]Krapp, H. and Hengstenberg, R., "Estimation of self-motion by optic flow processing in single visual interneurons," *Nature*, Vol. 384, 1996, pp. 463–466.

[36]Hassenstein, B. and Reichardt, W., "Systemtheoretische Analyse der Zeit-, Reihenfolgen- und Vorzeichenauswertung bei der Bewegungsperzeption des Russelkafers Chlorophanus," *Zeitschrift Fur Naturforschung*, Vol. 11b, 1956, pp. 513–524.

[37]Egelhaaf, M., "Visual Afferences to Flight Steering Muscles Controlling Optomotor Responses of the Fly," *Journal of Comparative Physiology A*, Vol. 165, No. 6, 1989, pp. 719–730.

[38]Shoemaker, P., O'Carroll, D., and Straw, A., "Velocity constancy and models for wide-field visual motion detection in insects," *Biological Cybernetics*, Vol. 93, No. 4, 2005, pp. 275–287.

[39]Lindemann, J., Kern, R., van Hateren, J., Ritter, H., and Egelhaaf, M., "On the computations analyzing natural optic flow: Quantitative model analysis of the blowfly motion vision pathway," *Journal of Neuroscience*, Vol. 25, No. 27, 2005, pp. 6435–6448.

[40]Neumann, T., "Modeling insect compound eyes: Space-variant spherical vision," *Biologically Motivated Computer Vision, Proceedings*, Vol. 2525, Springer-Verlag, Berlin, 2002, pp. 360–367.

[41]Buchner, E., "Behavioral analysis of spatial vision in insects," *Photoreception and vision in invertebrates*, edited by M. Ali, Plenum Press., New York, 1984, pp. 561–621.

[42]Howard, J., Dubs, A., and Payne, R., "The dynamics of phototransduction in insects," *Journal of Comparative Physiology A*, Vol. 154, 1984, pp. 707–718.

[43]Derham, W., "Boyle Lecture for 1711," 1713.

[44]Pflugsteadt, H., "Die Halteren der Dipteren," *Z. Wiss Zool.*, 1912, pp. 1–59.

[45]Gnatzym, W., Grünert, U., and Bender, M., "Companoform sensilla of *Calliphora vicina* (Insecta Diptera) I. Topography," *Zoomorphology*, Vol. 106, 1987, pp. 312–319.

[46]Hengstenberg, R., "Mechanosensory control of compensatory head rolling during flight in the blowfly *Calliphora erythrocephala*," *Meig. J. Comp. Physiol. A.*, Vol. 163, 1988, pp. 151–165.

[47]Nalbach, G., "The Halteres of the blowfly *Calliphora*," *Journal of Comparative Physiology A*, Vol. 173, 1994, pp. 293–300.

[48]Fayyazuddin, A. and Dickinson, M., "Haltere afferents provide direct, electrotonic input to a steering motor neuron in the blowfly Calliphora," *Journal of Neuroscience*, Vol. 16, No. 16, 1996, pp. 5225–5232.

[49]Faust, R., "Untersuchungen zum halterenproblem," *Zool. Jahrb. Physiol.*, Vol. 63, 1952, pp. 325–366.

[50]Dickinson, M., "Haltere-mediated equilibrium reflexes of the fruit fly, Drosophila melanogaster," *Philos. Trans. R. Soc. Lond.*, Vol. 354, No. 1385, 1999, pp. 903–916.

[51]Sherman, A., *The integration of visual and haltere feedback in Drosophila flight control*, Ph.D. thesis, University of California, Berkeley, 2003.

[52]David, C., "Relationship between body angle and flight speed in free-flying Drosophila," *Physiological Entomology*, Vol. 3, No. 3, 1978, pp. 191–195.

[53]Dickson, W. and Dickinson, M., "The effect of advance ratio on the aerodynamics of revolving wings," *Journal of Experimental Biology*, Vol. 207, 2004, pp. 4269–4281.

[54]Sherman, A. and Dickinson, M., "Summation of visual and mechanosensory feedback in Drosophila flight control," *Journal of Experimental Biology*, Vol. 207, 2004, pp. 133–142.

[55]Humbert, J., *Bio-Inspired Visuomotor Convergence in Navigation and Flight Control Systems*, Ph.D. thesis, California Institute ofTechnology, 2005.

[56]von Philipsborn, A. and Labhart, T., "A Behavioral-Study of Polarization Vision in the Fly, Musca-Domestica," *Journal of Comparative Physiology a-Sensory Neural and Behavioral Physiology*, Vol. 167, No. 6, 1990, pp. 737–743.

[57]Götz, K., "Course-Control, Metabolism and Wing Interference During Ultralong Tethered Flight in Drosophila-Melanogaster," *Journal of Experimental Biology*, Vol. 128, 1987, pp. 35–46.